



School of Chemistry

Nanostructured surfaces for antimicrobial applications & investigating how CVD diamond deposition is affected by varying growth times and temperatures

Paul-Lee Cairns

This thesis is submitted in partial fulfilment of the requirements for the Honours Degree of Bsc at the University of Bristol

Supervisor: Paul May
Second Assessor: Neil Fox

Abstract:

Part 1:

With an increasing demand for new antimicrobial techniques due to antibiotic resistance, bactericidal surfaces have shown a promising solution. This report focuses on nanotextured surfaces which rely on a mechanical mechanism of death upon adhesion to reduce bacterial multiplication, in hopes to reduce antibiotic use. The main mechanism of death is through the stretching of the bacterial cell membrane to a point where it ruptures, causing the cell to lyse.

A wide range of bactericidal nanostructures can be found within nature, with many animals exhibiting a form of antimicrobial surface. An example of this is the cicada which has an array of organised nanocones across its wings, which have been found to kill bacteria.

Many different materials have been researched such as titanium and steel, alongside more novel materials such as gold with multiple different types of structure having also been reviewed. By using different techniques, nanostructures can be manipulated to a desired design and arrangement.

Currently, surface nanostructures are not widely used for their bactericidal properties, however, some companies have started adapting their products to do so. One such company is Sharlet AF™ which has various medical devices displaying a surface that mimics that of a shark, which is bactericidal.

Part 2:

Diamond is formed in nature under extreme temperatures and pressures, which can be reproduced in the form of high-pressure high-temperature (HPHT) crystal growth. Other methods of diamond growth can be employed in order to form polycrystalline films in contrast to the single crystals formed by HPHT growth, such as chemical vapour deposition (CVD).

Atomic force microscopy (AFM) can be employed to analyse the surface topography of samples, allowing for 2-dimensional and 3-dimensional images to be created. AFM imaging was used to compare average nanostructure height across various samples at different temperatures and growth times.

Acknowledgements:

I would like to thank my supervisor Paul May for his support throughout the year. I would also like to thank my family, especially my mum, for their continuous support in my studies. Furthermore, I would like to thank Maria Juszczak, Frank Wang, Sundar Muthuganesan and Shihui Qiao for being an amazing group to work with.

Table of Contents

Part 1: Nanostructured surfaces for antimicrobial applications.....	6
1. Introduction:.....	6
1.1. Bacterial classification:.....	6
1.2. Bacterial cell multiplication and biofouling:.....	6
1.3. Antibiotic Resistance:.....	7
2. Bactericidal surfaces in nature:.....	8
2.1. Lotus leaf:	8
2.2. Cicada wings:	9
2.3. Gecko skin.....	10
2.4. How bactericidal surfaces are measured:	11
3. Physical mechanism of bacterial death:	11
3.1. Stretching of the cell membrane:	11
3.2. Piercing of the cell membrane:.....	13
4. Formation of synthetic nanostructures:.....	14
4.1. Black silicon (bSi):.....	14
4.2. Aluminium alloys:	15
4.3. Titanium:	16
4.4. Gold:	16
4.5. Steel:.....	17
5. Modifications:	18
5.1. Diamond coating:.....	18
5.2. Surface termination:	18
6. Current Uses:	19
6.1. Current implementation of surface nanostructures	19
6.2. Potential issues:	19
7. Conclusion:	20
8. Bibliography:	21
Part 2: Investigating how CVD diamond deposition is affected by varying growth times and temperatures.....	23
1. Introduction:.....	23
1.1. HPHT diamond formation:.....	23
1.2. CVD diamond formation:.....	23
1.3. Method of deposition:	24
1.4. AFM Imaging:.....	25

2. Method:	26
3. Results and discussion:	27
3.1. How temperature affects diamond growth:	27
3.2. Roughness of CVD diamond samples:.....	28
3.3. How growth time affects diamond growth:	29
4. Conclusion:	30
5. Bibliography	31

Part 1: Nanostructured surfaces for antimicrobial applications.

1. Introduction:

1.1. Bacterial classification:

Bacteria can be effectively categorised into two main groups, Gram-negative and Gram-positive. This was discovered by Dr Hans Christian Joachim Gram in 1884 whilst working in a laboratory in Berlin researching methods of bacterial staining.¹ Based on using iodine and crystal violet, which is a triarylmethane dye, this method of staining is used to form a dye-iodine complex, that is not easily removed from the bacterial cell wall. Decolourisation can then be used to differentiate between the two types of bacteria. As gram-negative bacteria have a much thinner peptidoglycan bilayer, as depicted in Figure 1, more dye is removed when decolourising agents such as ethanol or acetone are added. The peptidoglycan layer is a polysaccharide consisting of two monosaccharides, N-acetylglucosamine (NAG) and N-acetylmuramic (NAM) cross-linked by a tetrapeptide which increases the structural integrity of the cell.² This results in a very distinguished staining of the two types of bacteria, allowing them to be easily classified.

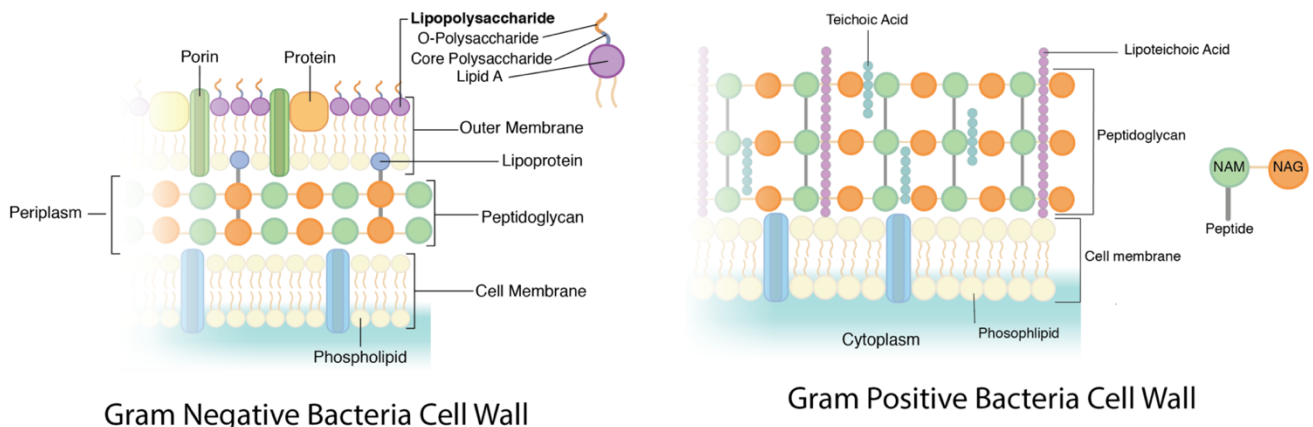


Figure 1: Simple diagrams depicting the larger peptidoglycan layer of Gram-positive bacterial cell walls alongside the lack of a lipopolysaccharide and protein layer.³

1.2. Bacterial cell multiplication and biofouling:

Bacterial infection starts soon after contact with surface tissue. They will begin to multiply and irreversibly attach to the surface through the formation of a biofilm, which is a matrix of extracellular polymers.⁴ This film consists of extracellular polymeric substances (EPS) which alongside extracellular DNA (eDNA) and carbohydrate-binding proteins form a three-dimensional cocoon-like structure as shown in Figure 2. Within this matrix, nutrients are

trapped and water is retained, which results in a satisfactory living environment for the bacteria.⁵ Composition of the EPS is altered based on changes in nutrient availability in the surroundings, allowing for the environment for bacteria within the matrix to be specifically tailored to different external stimuli.



Figure 2: A scanning electron microscope (SEM) image showing biofilm formation.⁴

Until the point of biofilm formation, the bacterial infection can be combatted relatively easily through the use of antibiotics, however, the biofilm acts as a barrier. The antibiotic can only affect the outermost parts of the film, but cannot reach the bacteria within.⁴ This whole process is termed biofouling and is the cause for many failed surgeries and implants. This is as biofilms are incredibly efficient at counteracting immune response.⁶ Biofilm formation on implants is a very complex issue as it can lead to a multitude of potentially life-threatening situations including chronic infection and device failure. Usually, high doses of antibiotics are used to combat the infection, else the implant is removed. However, removing the implant can be a very costly and risky procedure, alongside there being a high risk of re-infection.⁷

1.3. Antibiotic Resistance:

Antibiotics are currently the main combatant against bacterial infections, with penicillin being a popular choice against Gram-negative bacteria such as *Escherichia coli*. Using penicillin is a chemical way to destroy bacteria as it interrupts peptidoglycan synthesis which leads to weak points in the cell wall. This allows osmotic lysis to occur, which results in the rupturing of the cell.⁸ Antibiotic resistance is currently a serious problem throughout the world, being the main cause of death for an estimated 700,000 people per year as well

as millions of antibiotic-resistant caused infections.⁹ This is arguably caused by the overuse of antibiotics and since antibiotics are not an infinitely useful antimicrobial method, this increases the likelihood of bacteria adapting and become resistant.¹⁰

There are three main ways in which antibiotic resistance occurs; intrinsically, mutational and acquired.¹¹ Intrinsic resistance is where the bacteria already have a naturally occurring feature to combat the antibiotic mechanism. This includes producing enzymes to either protect themselves or deactivate the antibiotic. Mutational resistance is the chromosomal alteration in which an antibiotic resistant strain of the bacteria is produced. It is proposed that a single nucleotide base change can result in resistance, hence why the unnecessary overuse of antibiotics is dangerous. Lastly, acquired resistance is where the genetic information encoding antibiotic resistance is obtained through either transduction, transformation or conjugation. Transduction is the transfer of DNA between bacteria through the use of a bacteriophage whereas transformation is where the bacterium acquires this DNA which is free within the surroundings. Conjugation is the transfer of genetic information through cell-to-cell contact via a sex pilus or bridge, being the most common way antibiotic resistance is transferred.¹²

The ways in which bacteria are resistant to antibiotics are generally either by preventing the drug from reaching its target, altering the drug or deactivating the drug.¹¹ This, therefore, shows a requirement for a different approach to this problem, as it is evolving at a rate where new, effective antibiotics are becoming scarcer. One such way is the use of surface nanostructures, reducing the number of bacterial infections and could potentially be, when used in tandem with antibiotics, a start to the solution of this issue.

2. Bactericidal surfaces in nature:

Within nature, both antifouling and bactericidal properties are exhibited through the use of various nanotextured surfaces. A range of different nano-protrusions can be found throughout nature including needles, spinules and cones which all share the trait of using a mechanical mechanism to cause bacterial cell walls to rupture.¹³ Looking at these structures, biomimetic surfaces can be formed also showing similar properties.

2.1. Lotus leaf:

The lotus leaf exhibits antifouling properties, however, it does not actively kill bacteria so cannot be classed as bactericidal. Superhydrophobic effects are the driving force behind the antifouling properties of the lotus leaf, as when a water droplet falls on it, it quickly beads up and rolls off of the leaf. As it moves, the water droplet collects dirt, dust and bacterial cells. The nanosurface's superhydrophobic effects cause bacterial adhesion to be much more difficult. As a result of this, the lotus leaf is effectively a self-cleaning surface.¹⁴ Figure 3, taken from a review concerning superhydrophobicity of many different surfaces, shows that these properties are caused by the nanoscale topography of the lotus leaf. It is covered in an array of micropapillae which increases the contact angle of the water droplet and reduces sliding angle.¹⁵

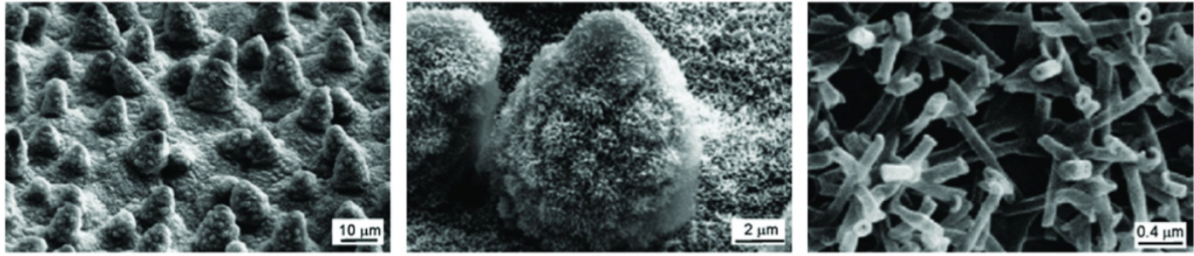


Figure 3: SEM images showing lotus leaf topography at different magnifications.¹⁵

2.2. Cicada wings:

One of the first bactericidal nanostructured surfaces researched in nature was that of the Cicada, a small species of winged insect. It was discovered that the topography of cicada wings is characterized by nanocones spaced roughly 170 nm apart with a base diameter of approximately 100 nm, tip diameter of 60 nm and a height of 200 nm in a hexagonal pattern (Figure 4).¹³

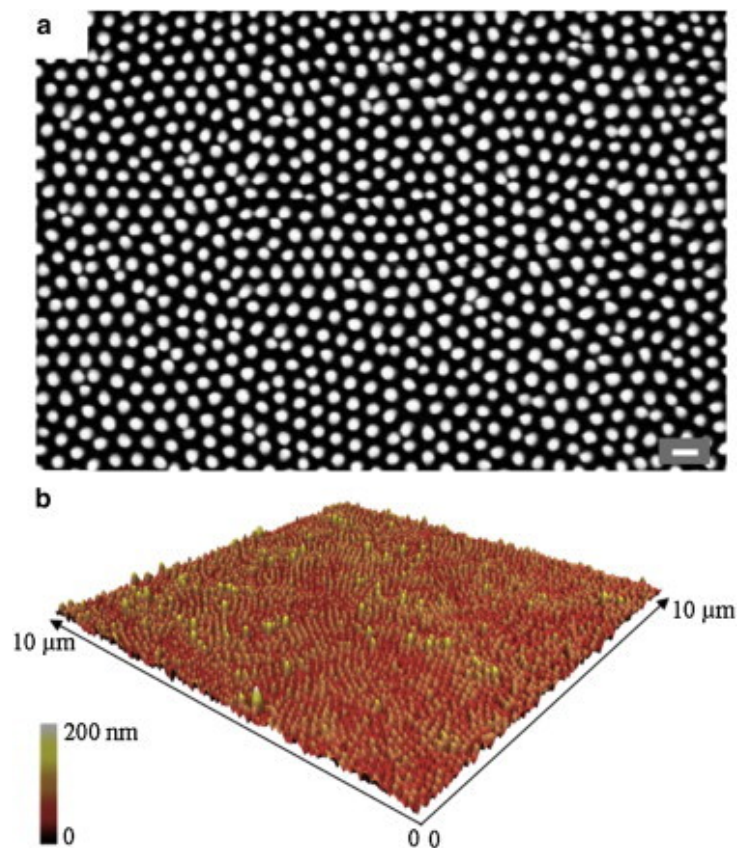


Figure 4: Surface topography of a cicada wing a) An electron micrograph of the surface of a cicada wing b) Representation of the topography of a cicada wing generated using data from an atomic force microscopy (AFM) scan.¹⁶

Studies of cicada wings have concluded that the two main factors affecting bactericidal ability are the hydrophobicity of the surface and the nanoprotusions. Figure 4a portrays the regular hexagon pattern of the nanoprotusions, with each pillar having 6 adjacent to itself. Paired with the relatively consistent heights of the nanopillars across the wing, as shown in Figure 4b, this shows a very uniform distribution of nano-protrusions throughout the surface.

Hydrophobicity has a large part to play as it has anti-biofouling properties, initially reducing the number of bacterial cells which can attach to the wing directly reducing the rate of biofilm formation.¹⁶ However, it has been found that even though rates of bacterial attachment is greatly decreased due to this, a small proportion of cells were able to attach. This is where the nanocones are incredibly useful as the small portion of bacteria which can attach, are mostly lysed due to the mechanical rupturing mechanism.¹⁷ Unfortunately since this mechanism is predominantly based on the low resistance of bacterial cells walls to the stress caused by nanostructure-induced stretching, Gram-positive bacteria have been shown to exhibit resistance to this.¹⁶

2.3. Gecko skin

Another similar surface is that of gecko skin. The surface is covered in curved spinules on the nanoscale having lengths of up to 4 microns, as shown in Figure 5. At the end of each spinule it is spherically capped, rather than sharp like a needle, suggesting a stretching mechanism for bacterial death as opposed to a puncturing one.¹⁸ Similar to the lotus leaf, gecko skin is also superhydrophobic. This results in much lower rates of bacterial adhesion and also the ability to self-clean. Due to the size of the structures, water droplets formed are able to go between the protrusions in order to remove dirt as well as dead and/or unadhered bacterial cells. As opposed to the lotus leaf which only uses this superhydrophobicity for antimicrobial purposes, the added nanostructures add even more resistance to bacterial adhesion.¹⁹ It has been found that the topography of gecko and cicada skin is very similar however the geckos' protrusions are spaced further apart. Due to the curvature of the spinules, the actual contact of these structures and bacterial cells is still very similar. Therefore, it is assumed that the mechanism of bacterial death is the same for both.¹⁸

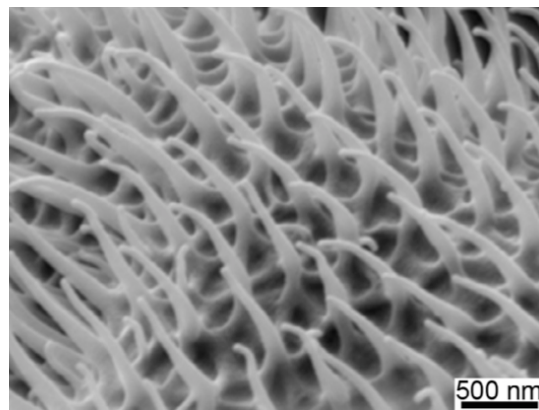


Figure 5: Scanning Electron Microscope (SEM) image showing the topography of gecko skin.¹⁸

2.4. How bactericidal surfaces are measured:

Antimicrobial susceptibility testing (AST) can be completed through the use of many different techniques. Arguably most common is the use of live/dead staining, allowing live and dead cells to be distinguished from each other and counted. This method uses two dyes, SYTO 9 and propidium iodide (PI), which differ in cell membrane permeability. SYTO 9 is able to cross all bacterial cell membranes, allowing for a complete cell count to be made when used alone whereas PI is only able to cross damaged membranes.²⁰ Therefore, PI is used as a counterstain in order to mark the dead cells as it cannot bind with living cells. The dyes are retained as they bind to nucleic acids in the nucleus with SYTO 9 producing a green fluorescence and PI red. By using fluorescence microscopy, the stained bacteria can be calculated to give the number of live/dead cells.²¹

Another similar method is the use of adenine triphosphate (ATP) bioluminescence, an effective biosensor which provides a real-time, sensitive assay. ATP is the major biological energy source so therefore reflects the existence of living microbes.²² This process relies on the luciferin-luciferase reaction, which requires ATP, forming oxyluciferin, an electronically excited compound. A photon is released as it returns to its ground state resulting in luminescence which can be measured by a Luminometer and expressed in relative light units (RLU), as it is directly proportional to the amount of ATP.²³

3. Physical mechanism of bacterial death:

3.1. Stretching of the cell membrane:

The first model to explain the interactions of bacterial cells and nanostructures was based on the deforming and rupturing of the cell wall. This is due to the nanostructures having heights greater than that of the bacterial cell wall, approximately 100 nm compared to 10 nm. Paired with the typical size of bacteria being roughly 500-1000 nm in length, the spacing between the nanopillars causes non-uniform stretching of the cell wall resulting in the cell rupturing.¹⁶ A mathematical model was proposed suggesting that the nanopillars do not pierce the cell wall, but rather the cell wall breaks due to stress caused by stretching between the pillars. This model can be summarised in Figure 6.

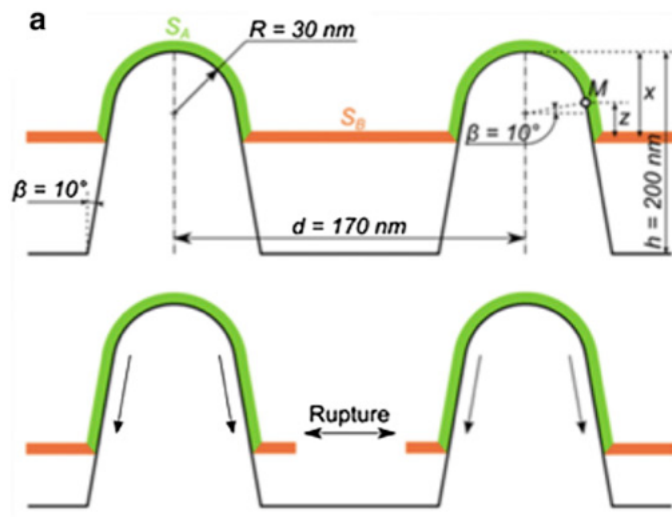


Figure 6: A simple diagram showing the rupturing of a bacterial cell wall due to stress caused by stretching between nanopillars.¹⁶

This shows that the surface adhered (S_A) to the nanostructures and the surface not (S_B), with the stretching degree being the difference in these areas. Once the stretching degree reaches a certain point, the cell wall will rupture. This model gives a relationship between layers of peptidoglycan and thickness of the cell wall being:

$$\gamma = \delta \times 1.03 \text{ nm}$$

Where γ represents cell wall thickness and δ the number of peptidoglycan layers. Using this relationship and the assumption of most gram-positive bacteria having 10-50 layers and gram-negative 1-3, their cell wall thicknesses are 30.9 nm and 2.06 nm respectively. With this information, by referring to Figure 7 we can predict maximum membrane stretch.²⁴

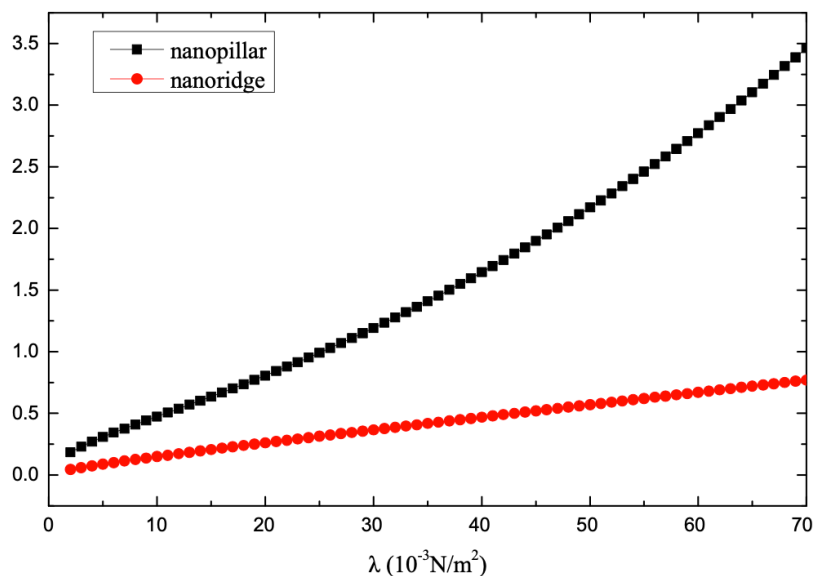


Figure 7: Graph showing how the maximum membrane stretching is related to cell size and type of surface nanostructure.²⁴

Figure 7 shows the correlation between cell size and the maximum the membrane can stretch before rupturing. There is a very clear trend, being maximum membrane stretching is proportional to cell size, as size increases so does maximum stretching. Therefore, with the cell wall thicknesses calculated for both types of bacteria, it is clear to see that Gram-positive bacteria have a larger maximum stretching amount and so are more resistant to cell lysis by the surface nanostructures.

3.2. Piercing of the cell membrane:

There is some disagreement however about the mechanism of death. The most widely accepted mechanism is that where the cell membrane is stretched between the nanoprotusions until it ruptures, however, others believe the bacterium is punctured by the structures. Another mechanism proposed is that the bacterial membrane is ruptured due to lateral movement of the cell whilst attached to the nanostructures.¹⁷ Whilst mention of the 3rd mechanism is scarce, the puncturing mechanism is referred to multiple times. A study was taken to see whether the nanoprotusions were piercing the cells or if they were just deforming the membrane. It was shown that both instances were correct, as shown in Figure 8.²⁵

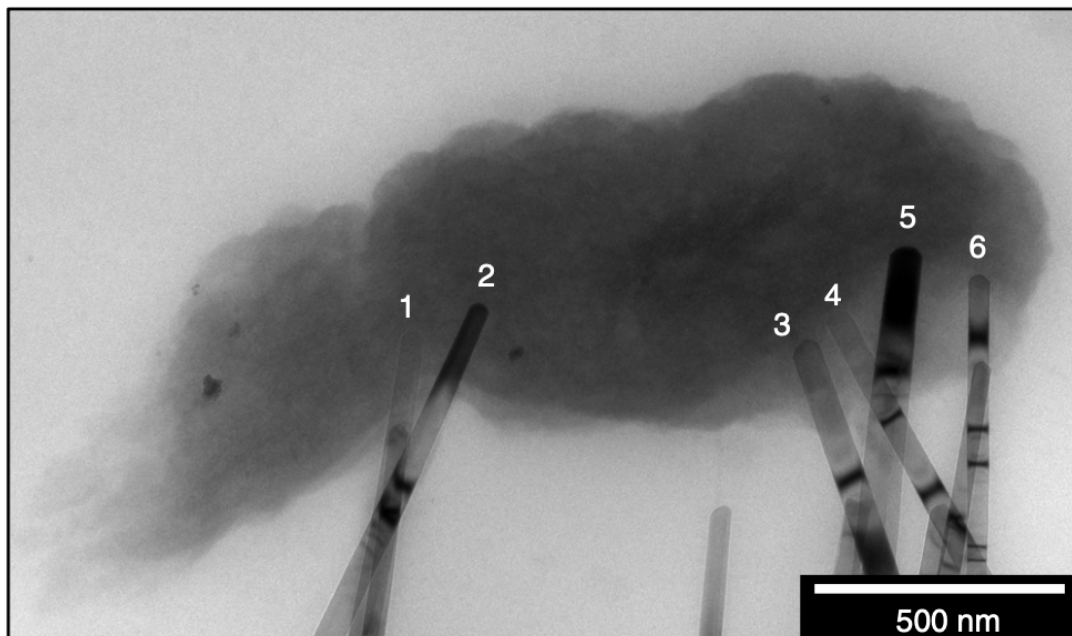


Figure 8: Bright-field transmission electron microscope (TEM) image showing structures 1-4 and 6 having penetrated the bacterium.²⁵

This shows that some of the nanopillars did in fact penetrate the bacterium. However, this was dependant on many parameters such as the strain of bacteria used, type of nanostructure and material of nanostructure. As a result of this, we cannot say that the mechanism of death is void of nanostructures piercing the membrane, however, the main mechanism is that of the membrane stretching.

4. Formation of synthetic nanostructures:

4.1. Black silicon (bSi):

Many biomimetic surfaces have been artificially created which show bactericidal properties. One popular material is black silicon (bSi) due to its antimicrobial and photovoltaic properties.²⁶ bSi is a nanomaterial with high aspect ratio, needle-like nanoprotusions and due to the roughness of the surface, very low reflection and very high light trapping effects are achieved giving a strong black appearance.²⁷ A popular method of bSi formation is through Reactive Ion Etching (RIE). This consists of a p-type boron-doped silicon wafer in a RIE chamber (Figure 9) with an inductively coupled radio frequency (RF) source which maintains a mixture of gases in a plasma state.²⁸ The mixture of gases used varies using different chlorine/fluorine compound derivatives, commonly SF_6 as well as O_2 .²⁹ Other gases can also be introduced giving different effects, such as CH_4 which is found to produce a more smooth etched, as opposed to a rough etched, surface. This however increases the amount of light reflected resulting in a surface that is not black.³⁰ Regarding SF_6 and O_2 , the majority of the etching occurs due to the formation of $\text{F}\cdot$ and $\text{O}\cdot$ radicals. $\text{F}\cdot$ etches the Si wafer and reacts forming unstable compounds of the form SiF_x which then further react with $\text{O}\cdot$ to form a SiO_xF_y passivation layer. This layer can then be etched via ion bombardment resulting in a competition between etching and passivation, forming the high aspect ratio nanostructures.²⁹

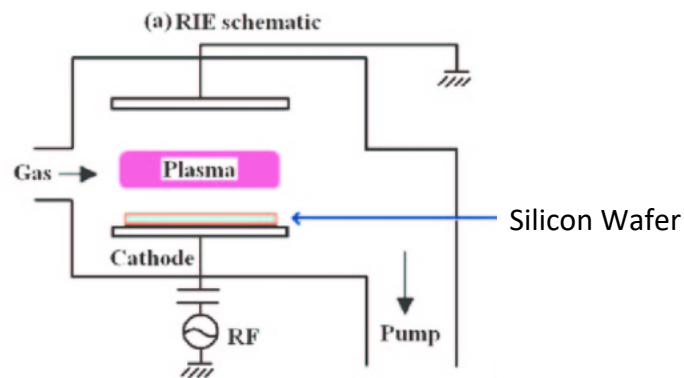


Figure 9: A schematic diagram of a RIE system for the etching of a silicon wafer.²⁸

4.2. Aluminium alloys:

Other surfaces which show bactericidal properties are etched aluminium alloys. Commonly used alloys include Al 1200/50502/6063 which are etched via a wet etching process. This method employs a strong base such as NaOH or KOH into which an aluminium plate is submerged in resulting in nano-sized ridges. Once sufficient etching has occurred, the plates are rinsed and sonicated in deionised water to prevent unwanted etching.³¹ It has been shown that these ridges exhibit anti-microbial properties through a similar physical method, straining bacterial cell walls causing them to lyse, as well as reducing attachment of the cells to the surface. An interesting point of research is the effect of these surfaces on the SARS-CoV-2 virus. The results of this research concluded that as well as being effective against gram-negative/positive bacteria they also decrease the time of which SARS-CoV-2 can survive as shown in Figure 10.³²

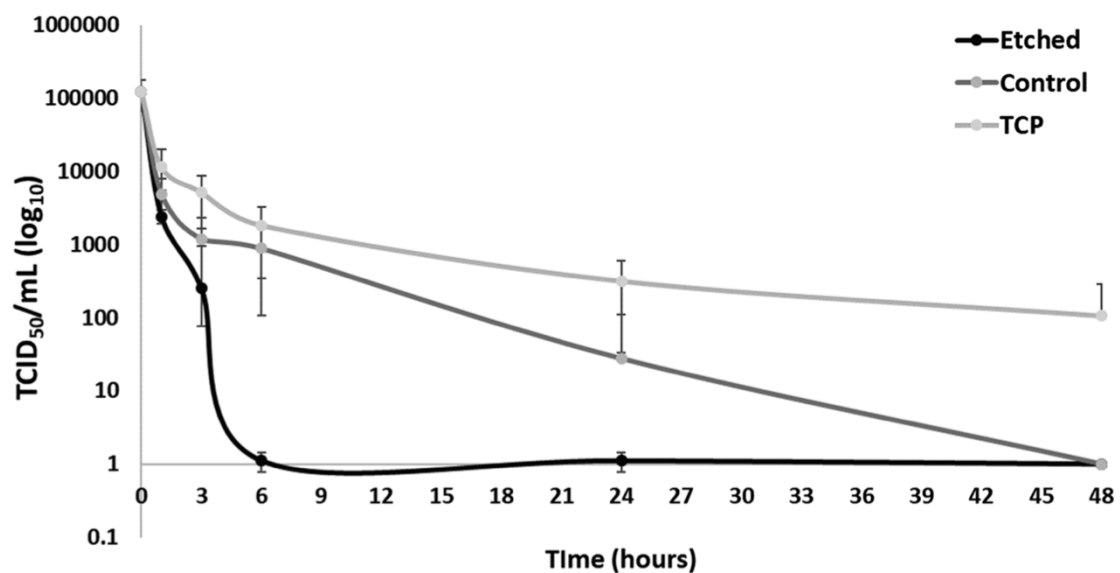


Figure 10: Graph showing the viability of SARS-CoV-2 virus on etched Al 6063 alloy, non-etched Al 6063 alloy and tissue culture plates (TCP).³²

This very clearly shows that the SARS-CoV-2 virus is much less viable to survive on the nanotextured Al surface compared to the flat, untreated one. The tissue culture infectious dose (TCID₅₀) is one way of calculating the number of infectious virus particles and is a logarithmic scale.³³ It's shown that at the 6-hour interval the TCID₅₀ is approximately 1 whereas on the non-etched surface it is approximately 1000. The time at which the non-etched surface reaches a TCID₅₀ of 1 is 48 hours after exposure, showing an 8x increase in antimicrobial effects by the etched surface.

4.3. Titanium:

A promising area of research is the use of protruding nanostructures on titanium and its alloys through a simple Thermal Oxidation (TO) process within a carbon-containing atmosphere. This is undertaken at high temperatures which range from 400-900 °C forming a TiO₂ core covered by a carbon shell. The carbon shell displays superhydrophobic properties, reducing bacterial adhesion and further biofilm formation.³⁴ It has been shown that the nanoprotusions formed mimic that of the dragonfly wing, with nanospikes having a diameter of 20 nm and heights of 1-2 μm.³⁵ RIE can also be used for titanium however TO is relatively simple and low-cost.

Another way to form titanium nanostructures is through Glancing Angle Deposition (GLAD) which allows for a high degree of precision in controlling nanostructure design, distribution and height. It has been used to create a biomimetic surface resembling the cicada wing with nanospikes of uniform spacing and heights.³⁴ The GLAD method is more complex as it is based upon a vapour source being at an oblique angle to a substrate which can be moved to manipulate deposition and therefore structure growth.³⁶ Due to ballistic shadowing, as shown in Figure 11, controlling the incident angle of the vapour and rotation of the substrate allows for very precise growth of the nanostructures.³⁷

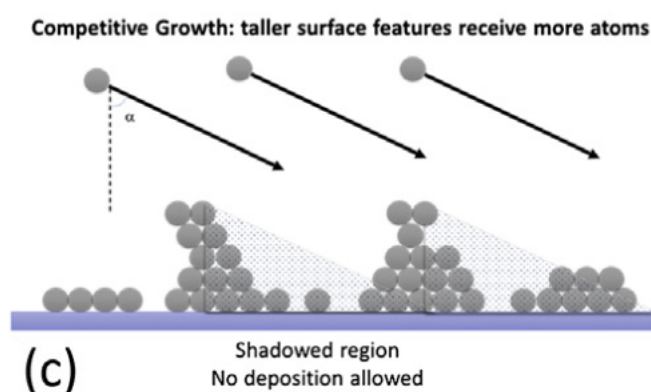


Figure 11: Diagram representing how ballistic shadowing is used to manipulate nanostructure growth.³⁷

4.4. Gold:

Gold nanostructures have also been formed using various designs such including nanopillars, nanorings and nanonuggets (Figure 12) with their bactericidal abilities being compared. These differing patterns were formed by the electrodeposition of gold onto nanoporous alumina plates. First, a conducting layer of tungsten is deposited onto a silicon wafer, with an aluminium layer being deposited on top of this. The aluminium layer is then anodised in a phosphoric acid solution, with the oxidation of aluminium forming organised nanopore structures. After being rinsed with deionised water the sample is dried and, by using the tungsten layer as the electrode, gold is electrodeposited into the nanocavities. Finally, selective dissolving of the alumina layer exposes the gold nanostructures.³⁸

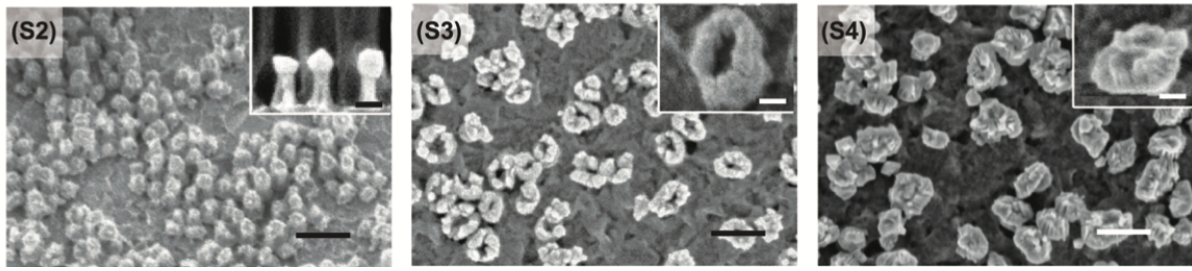


Figure 12: SEM images showing different types of gold nanostructure S2) nanopillars S3) nanorings S4) nanonuggets.³⁸

In order to create the desired nanoring and nanonugget patterns, the alumina surfaces are first selectively etched using SF₆ plasma. This demonstrates the ability to create nanostructures in many different desired patterns/arrangements. The different arrangements of the gold nanopillars seemed to not influence antimicrobial properties very much at all, with the number of viable cells at the end of the test ranging from approximately 10-100 as opposed to the range of 10⁵-10⁶ on the flat test surfaces.³⁸

4.5. Steel:

The last material that will be discussed is steel, in particular the popular alloy stainless steel. Nanostructures can also be formed on the steel surface via the use of femtosecond lasers, creating a surface with topographical similarities to the lotus leaf.³⁹ This process works by irradiating the stainless-steel surface with femtosecond laser pulses with circular or linear polarisation. Since this leaves surface structure mimetic to that of the lotus leaf, this is said to be antifouling as opposed to bactericidal as the structures do not actively kill bacteria. Studies into nanostructured steel have shown significant antifouling properties compared to the flat test counterpart, with a significant decrease in adhered cells being observed.²⁵ A decrease in ease of attachment, therefore decreased biofilm formation, is effective however compared to other surfaces which exhibit similar properties as well as the active mechanical death mechanism, this seems like a lesser alternative. However, with the wide array of uses of stainless steel, having an antifouling surface may be beneficial.

5. Modifications:

5.1. Diamond coating:

These nanostructures can be modified in various ways to change their properties. Popular desired characteristics for these structures are strength and durability. Surfaces such as bSi which, due to its high aspect ratio nanoprotusions, are very brittle and are damaged using minute force.⁴⁰ To combat this, the surface can be coated in a diamond film that increases both the strength and durability of the structures. The diamond coating of bSi leads to what is known as black diamond (bD).

One way of creating this film is through the use of diamond seeding where a suspension of detonation nanodiamond (DND) in methanol is deposited onto the surface via an electrospray process.⁴⁰ This results in a coating of DND seeds on the bSi, which can then be placed in a hot filament chemical vapour deposition (HFCVD) chamber. Heavily boron-doped micro/nanocrystalline diamond (MCD and NCD respectively) is also placed in the chamber, which is then deposited onto the surface forming a diamond film. It has been found that using NCD results in the bD needles being more rounded and the spacings between the needles start to be filled in depending on growth time. In regard to bactericidal properties, using MCD gave 'sharper' needles which would in theory pierce bacterial cell walls more easily, hence why this may be a preferred method.⁴⁰ Further modifications can also be employed to increase the antimicrobial properties, one being changing surface hydrophobicity.

5.2. Surface termination:

Alongside the mechanical mechanism of bacterial death, surface chemistry provides an even less favourable environment for bacterial attachment and subsequent biofouling/biofilm formation. One way in which hydrophobicity is controlled is through the different compounds which can be used to terminate the diamond film. Without further termination, the diamond film on bD is usually hydrogen terminated however through the use of plasma treatment this can be easily modified. Chemical termination using O, NH₂ and F were studied finding F termination resulted in a superhydrophobic surface.⁴¹ As the percentage of bacteria adhering to the surface decreases with increasing hydrophobicity, having a superhydrophobic further reduces the probability of a biofilm to form if the mechanical mechanism fails. A study has shown that fluorine terminated bD can reduce bacterial adhesion by up to 50%.⁴¹

6. Current Uses:

6.1. Current implementation of surface nanostructures

Currently, nanostructured surfaces are not widely used for their bactericidal properties. Some companies however are implementing this into their products. One such company is Sharklet AF™ who have already incorporated a biomimetic shark skin surface onto various medical devices including urinary catheters, endotracheal tubes, wound dressings and central venous catheters.³⁴ There have been concerns however that the increased bactericidal properties of implants could lead to increased bacterial growth on surrounding tissue. This is a problem for many reasons. Firstly, this increased bacterial growth may cause the body to reject the implant at higher rates due to the body's immune system, causing complications regarding extraction and re-insertion of the implant. Furthermore, this leads to an increased risk of local inflammation and the spreading of the infection potentially leading to chronic infection, and in severe cases amputation or even death.

6.2. Potential issues:

There are more potential issues which arise with the use of nanotextured surfaces for their antimicrobial effects. It has been shown that the needle-like nanoprotrusions are susceptible to snapping when only a small amount of force is applied.⁴⁰ This raises the question of if these structures would be able to withstand the body's environment, as well as if the snapped pieces pose a health risk. Extensive research into nanoparticles has been undertaken showing many issues when using them within the body. For example; ZnO nanoparticles have been shown to cause cell shrinkage and decreased mitochondrial function, CuO/Al₂O₃ nanoparticles cause oxidative stress, TiO₂ has been shown to cause liver damage in rats and Ag and Fe have been found to be toxic to the human body.³⁹ These are all very serious issues which need to be investigated before wider implementation of nanostructures can be introduced.

7. Conclusion:

The plethora of fabrication methods and materials used show how varied this field can be and can cater to many different needs. The precision of nano design and ability to alter layout, height, width and shape etc further allows for these structures to be tailor-made for their specific purpose. Alongside this, with relatively low-cost and simple methods now in place the feasibility of mass-producing is heightened, and it is likely they will be more commonly used in the future. Especially during the recent worldwide events involving COVID-19 which highlighted the importance of antimicrobial efforts. Some of the methods mentioned are potentially too novel to be widely used such as bSi/bD and gold however since titanium, aluminium and steel are already heavily embedded into society, there is good reason for this to be further explored. With more research being done into the potential harmful effects, I believe that using nanotextured surfaces for their bactericidal properties has a good chance of being a viable alternative to the use of antibiotics. This is due to the fact that if fewer bacterial infections occur originally, in theory, less antibiotics will need to be used, hopefully slowing antibiotic resistance and being a better, more long-term solution to this problem.

8. Bibliography:

1. M. Peck and T. Badrick, *Journal of Histotechnology*, 2017, **40**, 54-61.
2. T. J. Beveridge and J. A. Davies, *Journal of Bacteriology*, 1983, **156**, 846-858.
3. L. Bruslind, *General Microbiology*, Oregon State University, 2020, ch. 4, pp. 33-34.
4. R. M. Donlan, *Clinical Infectious Diseases*, 2001, **33**, 1387-1392.
5. M. Kostakioti, M. Hadjifrangiskou and S. J. Hultgren, *Cold Spring Harbor Perspectives in Medicine*, 2013, **3**, 23.
6. G. D. Bixler and B. Bhushan, *Philosophical Transactions of the Royal Society a-Mathematical Physical and Engineering Sciences*, 2012, **370**, 2381-2417.
7. Z. Khatoon, C. D. McTiernan, E. J. Suuronen, T. F. Mah and E. I. Alarcon, *Heliyon*, 2018, **4**, 36.
8. G. M. S. Soares, L. C. Figueiredo, M. Faveri, S. C. Cortelli, P. M. Duarte and M. Feres, *Journal of Applied Oral Science*, 2012, **20**, 295-309.
9. H. O. Ukuhor, *Journal of Infection and Public Health*, 2021, **14**, 53-60.
10. C. L. Ventola, *P & T : a peer-reviewed journal for formulary management*, 2015, **40**, 277-283.
11. J. M. Munita and C. A. Arias, *Microbiology Spectrum*, 2016, **4**, 24.
12. C. J. H. von Wintersdorff, J. Penders, J. M. van Niekerk, N. D. Mills, S. Majumder, L. B. van Alphen, P. H. M. Savelkoul and P. F. G. Wolffs, *Frontiers in Microbiology*, 2016, **7**, 10.
13. A. Tripathy, P. Sen, B. Su and W. H. Briscoe, *Advances in Colloid and Interface Science*, 2017, **248**, 85-104.
14. Z. H. Li and Z. G. Guo, *Nanoscale*, 2019, **11**, 22636-22663.
15. M. A. Samaha, H. V. Tafreshi and M. Gad-el-Hak, *Comptes Rendus Mecanique*, 2012, **340**, 18-34.
16. S. Pogodin, J. Hasan, V. A. Baulin, H. K. Webb, V. K. Truong, T. H. P. Nguyen, V. Boshkovikj, C. J. Fluke, G. S. Watson, J. A. Watson, R. J. Crawford and E. P. Ivanova, *Biophysical Journal*, 2013, **104**, 835-840.
17. J. Roman-Kustas, J. B. Hoffman, J. H. Reed, A. E. Gonsalves, J. Oh, L. N. Li, S. M. Hong, K. D. Jo, C. E. Dana, N. Miljkovic, D. M. Cropek and M. Alleyne, *Advanced Materials Interfaces*, 2020, **7**, 11.
18. G. S. Watson, D. W. Green, L. Schwarzkopf, X. Li, B. W. Cribb, S. Myhra and J. A. Watson, *Acta Biomaterialia*, 2015, **21**, 109-122.
19. J. Riedel, M. J. Vucko, S. P. Blomberg and L. Schwarzkopf, *Ecology and Evolution*, 2020, **10**, 4640-4651.
20. J. Robertson, C. McGoverin, F. Vanholsbeeck and S. Swift, *Frontiers in Microbiology*, 2019, **10**, 13.
21. M. Rosenberg, N. F. Azevedo and A. Ivask, *Scientific Reports*, 2019, **9**, 12.
22. Z. A. Khan, M. F. Siddiqui and S. Park, *Diagnostics*, 2019, **9**, 17.
23. H. R. Eed, N. S. Abdel-Kader, M. H. El Tahan, T. H. Dai and R. Amin, *Journal of Sensors*, 2016, **2016**, 5.
24. F. D. Xue, J. J. Liu, L. F. Guo, L. R. Zhang and Q. Z. Li, *Journal of Theoretical Biology*, 2015, **385**, 1-7.
25. J. Jenkins, J. Mantell, C. Neal, A. Gholinia, P. Verkade, A. H. Nobbs and B. Su, *Nature Communications*, 2020, **11**, 14.

26. E. P. Ivanova, J. Hasan, H. K. Webb, G. Gervinskis, S. Juodkazis, V. K. Truong, A. H. F. Wu, R. N. Lamb, V. A. Baulin, G. S. Watson, J. A. Watson, D. E. Mainwaring and R. J. Crawford, *Nature Communications*, 2013, **4**, 7.
27. M. Otto, M. Algasinger, H. Branz, B. Gesemann, T. Gimpel, K. Fuchsel, T. Kasebier, S. Kontermann, S. Koynov, X. P. Li, V. Naumann, J. Oh, A. N. Sprafke, J. Ziegler, M. Zilk and R. B. Wehrspohn, *Advanced Optical Materials*, 2015, **3**, 147-164.
28. H. Ji, J. Choi, G. Lim, B. Parida, K. Kim, J. H. Jo and H. S. Kim, *Journal of Nanoscience and Nanotechnology*, 2013, **13**, 7806-7813.
29. X. G. Liu, P. R. Coxon, M. Peters, B. Hoex, J. M. Cole and D. J. Fray, *Energy & Environmental Science*, 2014, **7**, 3223-3263.
30. R. Legtenberg, H. Jansen, M. Deboer and M. Elwenspoek, *Journal of the Electrochemical Society*, 1995, **142**, 2020-2028.
31. J. Hasan, S. Jain, R. Padmarajan, S. Purighalla, V. K. Sambandamurthy and K. Chatterjee, *Materials & Design*, 2018, **140**, 332-344.
32. J. Hasan, A. Pyke, N. Nair, T. Yarlagadda, G. Will, K. Spann and P. Yarlagadda, *ACS Biomaterials Science & Engineering*, 2020, **6**, 4858-4861.
33. S. J. Smither, C. Lear-Rooney, J. Biggins, J. Pettitt, M. S. Lever and G. G. Olinger, *Journal of Virological Methods*, 2013, **193**, 565-571.
34. M. I. Ishak, X. Y. Liu, J. Jenkins, A. H. Nobbs and B. Su, *Coatings*, 2020, **10**, 19.
35. C. M. Bhadra, V. K. Truong, V. T. H. Pham, M. Al Kobaisi, G. Seniutinas, J. Y. Wang, S. Juodkazis, R. J. Crawford and E. P. Ivanova, *Scientific Reports*, 2015, **5**, 12.
36. N. Ziegler, C. Sengstock, V. Mai, T. A. Schildhauer, M. Koller and A. Ludwig, *Nanomaterials*, 2019, **9**, 11.
37. A. Barranco, A. Borrás, A. R. Gonzalez-Elipe and A. Palmero, *Progress in Materials Science*, 2016, **76**, 59-153.
38. S. M. Wu, F. Zuber, J. Brugger, K. Maniura-Weber and Q. Ren, *Nanoscale*, 2016, **8**, 2620-2625.
39. A. Jaggessar, H. Shahali, A. Mathew and P. K. D. V. Yarlagadda, *Journal of Nanobiotechnology*, 2017, **15**.
40. P. W. May, M. Clegg, T. A. Silva, H. Zanin, O. Fatibello, V. Celorrio, D. J. Fermin, C. C. Welch, G. Hazell, L. Fisher, A. Nobbs and B. Su, *Journal of Materials Chemistry B*, 2016, **4**, 5737-5746.
41. O. Dunseath, E. J. W. Smith, T. Al-Jeda, J. A. Smith, S. King, P. W. May, A. H. Nobbs, G. Hazell, C. C. Welch and B. Su, *Scientific Reports*, 2019, **9**, 10.

Part 2: Investigating how CVD diamond deposition is affected by varying growth times and temperatures.

1. Introduction:

1.1. HPHT diamond formation:

Diamond has a set of unique properties which are desirable for scientific and industrial processes, including being extremely durable and having an incredibly high melting point. These properties are attributable to the carbon-carbon sp^3 bonding where each carbon atom is bonded to four others in a regular tetrahedral arrangement.¹ There are many ways in which diamond can be grown such as under High-Pressure High-Temperature (HPHT) conditions and through Chemical Vapour Deposition (CVD). High-pressure crystallisation relies on the catalytic ability of graphite to be converted into diamond in a specialised chamber under extreme conditions in the realm of approximately 1500-1900 °C and 7 GPa.² Crystals are then formed due to the thermodynamic stability of the diamond.

Different catalysts can be used during this process, commonly being transition metal based. The use of more exotic compounds, both metals and non-metals, are able to produce crystals with unusual properties such as semiconducting diamonds which are doped with phosphorous.² Besides the extreme conditions required and the long growth times, another issue with HPHT crystal growth is the fact that it produces singular diamond crystals as opposed to a film, limiting its uses.³

1.2. CVD diamond formation:

Another method for the formation of diamond is CVD. This process relies on the excitation of gas-phase carbon-containing molecules which undergo reactions on the deposition surface to build up a diamond film. Excitation of the gaseous molecules can be done in a variety of ways such as thermal activation via a hot filament or oxyacetylene torch, or electrical discharge via R.F., D.C. and microwave.⁴ It has been found that the preferred concentration of carbon, commonly CH_4 , in the gaseous mixture is less than 2% with the remaining gas being composed of hydrogen. Conditions within the CVD reactor are important as too high or low of a temperature can cause graphitic compounds to form.⁴ A common CVD technique is Hot Filament CVD (HFCVD) as it is a cheap, relatively simple way to produce polycrystalline diamond films of reasonable quality. A simple HFCVD reactor is depicted in Figure 1.

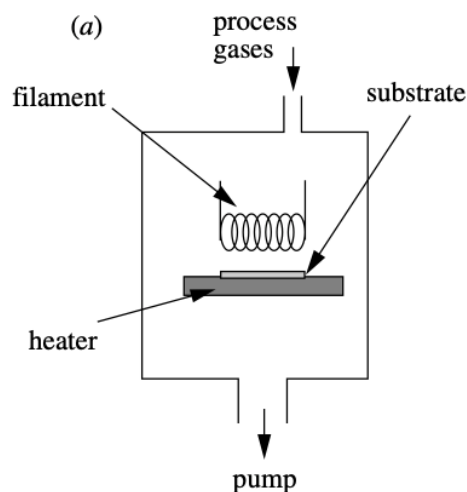


Figure 1: A simple diagram depicting a HFCVD reaction chamber.³

This process is low-pressure, so pumps maintain an environment of approximately 0.03 atm and a temperature of 700-900 °C. The substrate to be deposited on, for example Si, is placed below a filament which is heated to over 2200 °C.³ Therefore, the filament excites the gaseous mixture allowing for deposition.

1.3. Method of deposition:

It was initially thought that the main reactive hydrocarbon radical involved in diamond growth was $\text{CH}_3\cdot$, shown in Figure 2, however, it has been found that other hydrocarbon radicals may play a role.⁵

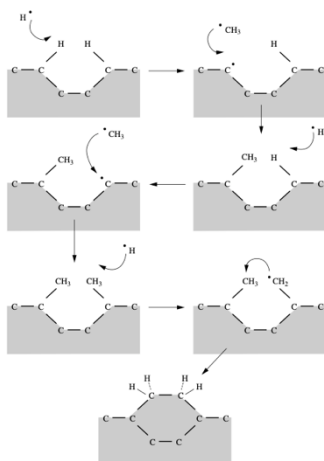


Figure 2: Schematic of the addition of CH_3 onto the substrate surface, leading to diamond growth.³

Most mechanisms describe atomic hydrogen removing surface hydrogen atoms leaving monoradical sites to which a $\text{CH}_3\cdot$ radical can bond with. This process then occurs on a neighbouring carbon atom. One of the exposed CH_3 groups then loses a H atom through the

bonding of atomic hydrogen, leaving a $\text{CH}_2\cdot$ radical site. This radical can then bond with the neighbouring CH_3 , with this process repeating causing the build-up of the diamond lattice. Different radical surface sites are formed, however, being monoradical and biradical with important sites shown in Figure 3.

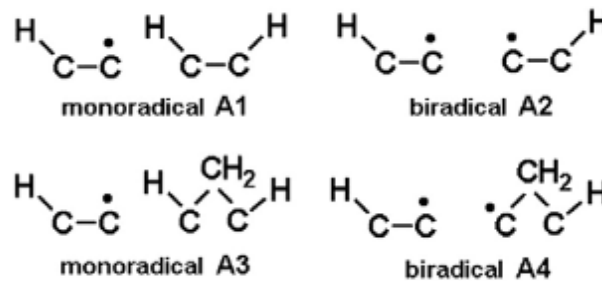


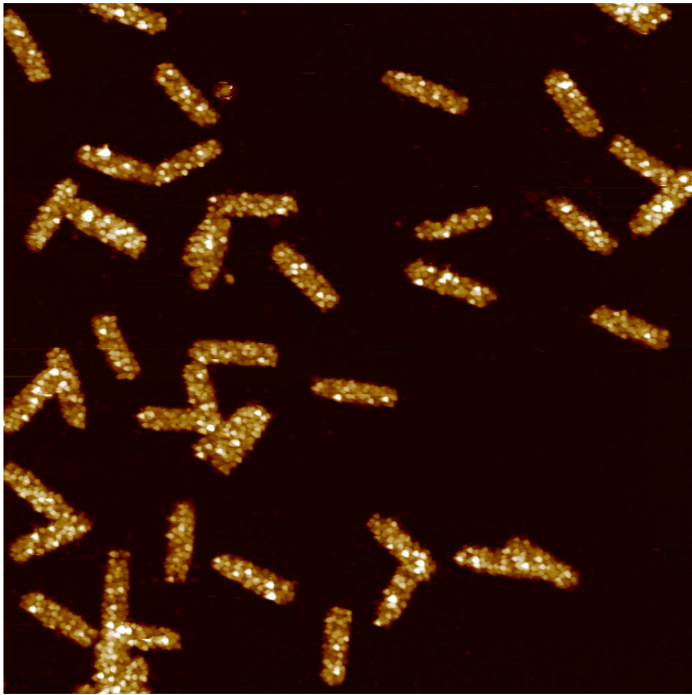
Figure 3: Important radical surface sites for CVD diamond growth.⁵

This model suggests the primary process in which the diamond layer is deposited is through the biradical surface sites. However, in addition to this, monoradical sites are also utilised. This is by the $\text{CH}_3\cdot$ bonding to the vacant site, and if a neighbouring carbon atom loses a H atom via bonding to atomic hydrogen, a bridge can form between the new vacant site incorporating the CH_3 into the lattice.⁵

1.4. AFM Imaging:

A way in which the formed diamond nanostructures can be measured is through the use of Atomic Force Microscopy (AFM). AFM is a spectroscopic technique which utilises a micro-cantilever that is moved across the sample, with there being 3 modes of use; non-contact, contact and tapping.⁶ The forces produced by the topography of the surface onto the cantilever are monitored allowing for a 3-dimensional representation of the surface to be generated. When used in contact mode, as the tip is brought closer to the surface, attractive forces caused the cantilever to deflect towards the surface. However, as the tip is brought even closer to the surface and makes contact, repulsive forces cause the cantilever to deflect away from the surface.⁷ A laser beam is deflected off of the cantilever onto a Position Sensitive Photo Detector (PSPD) so as the cantilever deflects the laser, these movements are detected. Therefore, as the cantilever passes over a surface structure, the reflected beam changes position on the PSPD and is able to be used to generate an image. A feedback loop is used to control the height of the tip above the surface in order to maintain a constant laser position.⁷ When used in non-contact mode, the cantilever oscillates slightly above the sample surface and an image is generated through a similar method. Tapping mode combines both of these techniques, oscillating the cantilever above the surface allowing the tip to make contact for a minimal amount of time.⁶ This results in the generation of both 2-dimensional and 3-dimensional images of the surface topography, as shown in Figure 3.

a)



b)

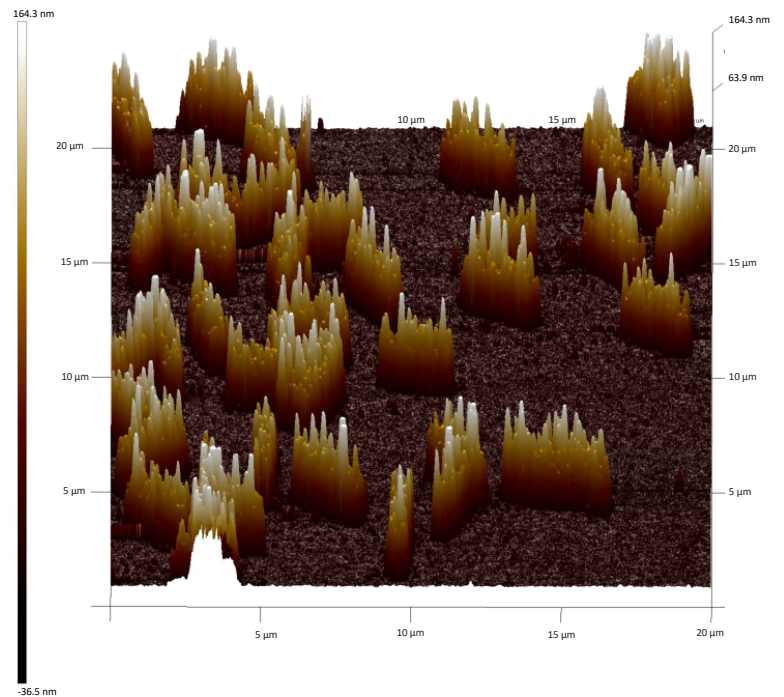


Figure 4: AFM images showing a) 2-dimensional b) 3-dimensional representations of the topography of the CVD diamond grown surface.

Figure 3 is an example of one of the samples which were scanned via AFM. 3a is a 2-dimensional image depicting multiple separate particles, coloured in a way that indicates the different heights of peaks across each particle. As shown by the colour chart, lighter coloured areas show peaks of greater height. 3b is a 3-dimensional rendering of the surface topography, being coloured in a similar way to 3a. This forms a clearer image of individual peaks within a particle alongside relative heights throughout the sample.

2. Method:

Diamond was deposited onto 8 +/- 2 nm thick silicon wafers via a microwave plasma CVD (MPCVD) process using a methane concentration of 4% and power of 1250 W. These were completed for five different time intervals (5, 10, 20, 40 and 60 minutes) at six different temperatures (689.6, 740.6, 845.8, 969, 1067.25 and 1075.4 °C). Once produced, these samples were analysed via AFM imaging, and further analysed using the computer software Nanoscope. Each particle was examined to conclude an average nanostructure height per sample, producing graphs from which trends in diamond deposition could be determined.

3. Results and discussion:

3.1. How temperature affects diamond growth:

Figure 4 shows the relationship between nanostructure height and temperature at a growth time of 3 minutes. It clearly shows that the nanostructures with the highest average height were present at the lowest temperature, being 264.01 nm at 689.6 °C. The lowest average height was 54.51 nm at a temperature of 1067.25 °C. The error bars for each point are shown as standard deviations, communicating the differences in nanostructure heights per sample with a large standard deviation showing a large variation in nanostructure height.

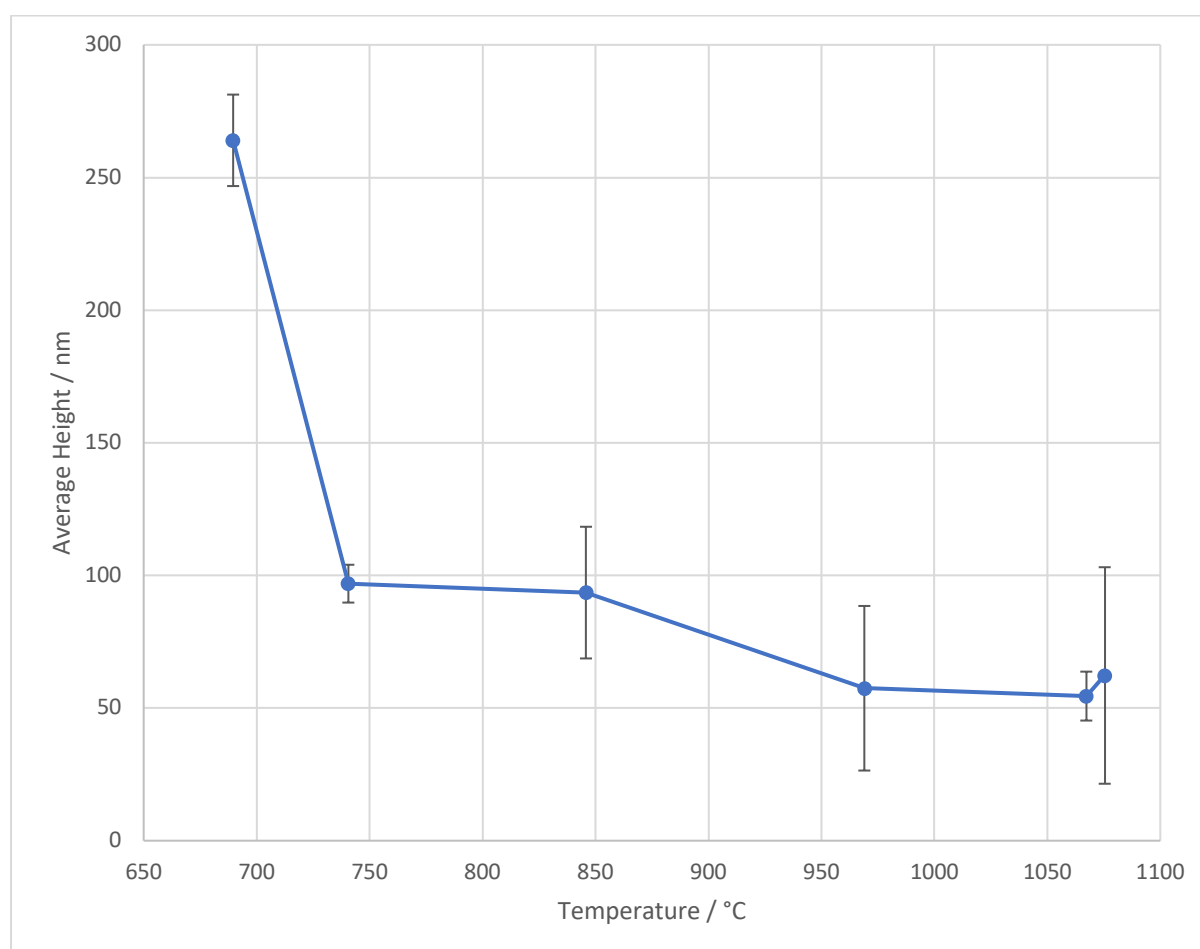


Figure 5: Scatter graph showing the average height of nanostructures against temperature at a growth time of 3 minutes with associated error bars depicting the standard deviation of the data point.

It is theorised that at lower temperatures aromatic hydrocarbons can condensate onto the available carbon sp^3 sites, hindering diamond growth. These aromatic molecules are then thought to be converted into a sp^2/sp^3 carbon system.⁸ The building up of this carbonaceous structure could explain the initial large average heights when grown at low temperatures.

At increased temperatures, the $C_x\cdot$ radicals are the limiting kinetic factor due to their thermodynamic stability. Therefore, available sp^3 hybridised $C_x\cdot$ sites decompose forming sp^2 graphitic compounds. These graphitic portions are more readily etched than the diamond which is formed, hence only a small increase in structure height as opposed to the rapid decline at lower temperatures.⁸

3.2. Roughness of CVD diamond samples:

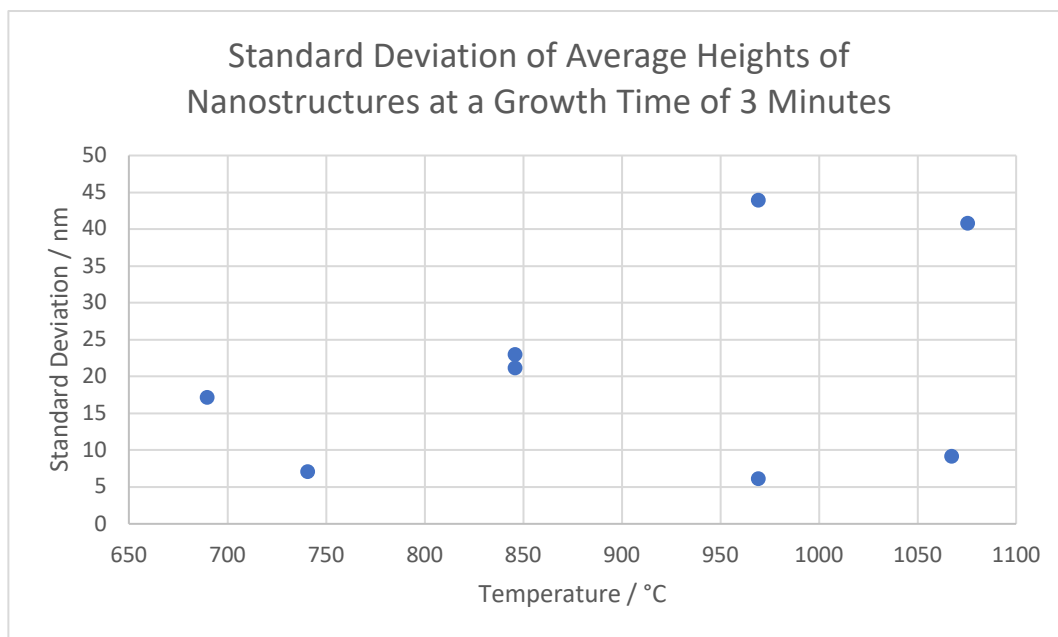


Figure 6: Graph showing standard deviations for average nanostructure heights at a growth time of 3 minutes.

Figure 5 shows how the standard deviations of nanostructure height vary according to changes in temperature. The temperatures 740.6 ° and 1067.25 °C all showed the lowest standard deviations, being 7.13 and 9.22 respectively. At 969 °C there were two samples, with standard deviations of 6.19 and 43.95, being 31.02 once sample data is combined. This shows a large difference between the uniformity of the structure heights in both samples. The sample with a standard deviation of 6.19 shows a much more constant height of the nanostructures whereas 43.95 shows a very varied set of heights. At 1075.4 °C the standard deviation is 40.81, also showing a very diverse set of nanostructure heights.

There is not an evident link between temperature and the consistency of nanostructure height, however, it could be argued that at higher temperatures there is greater surface roughness.

3.3. How growth time affects diamond growth:

The CVD process was undertaken at identical temperature intervals with differing growth times, being 3, 10, 20, 40 and 60 minutes. Graphs of average structure height are shown in Figure 6.

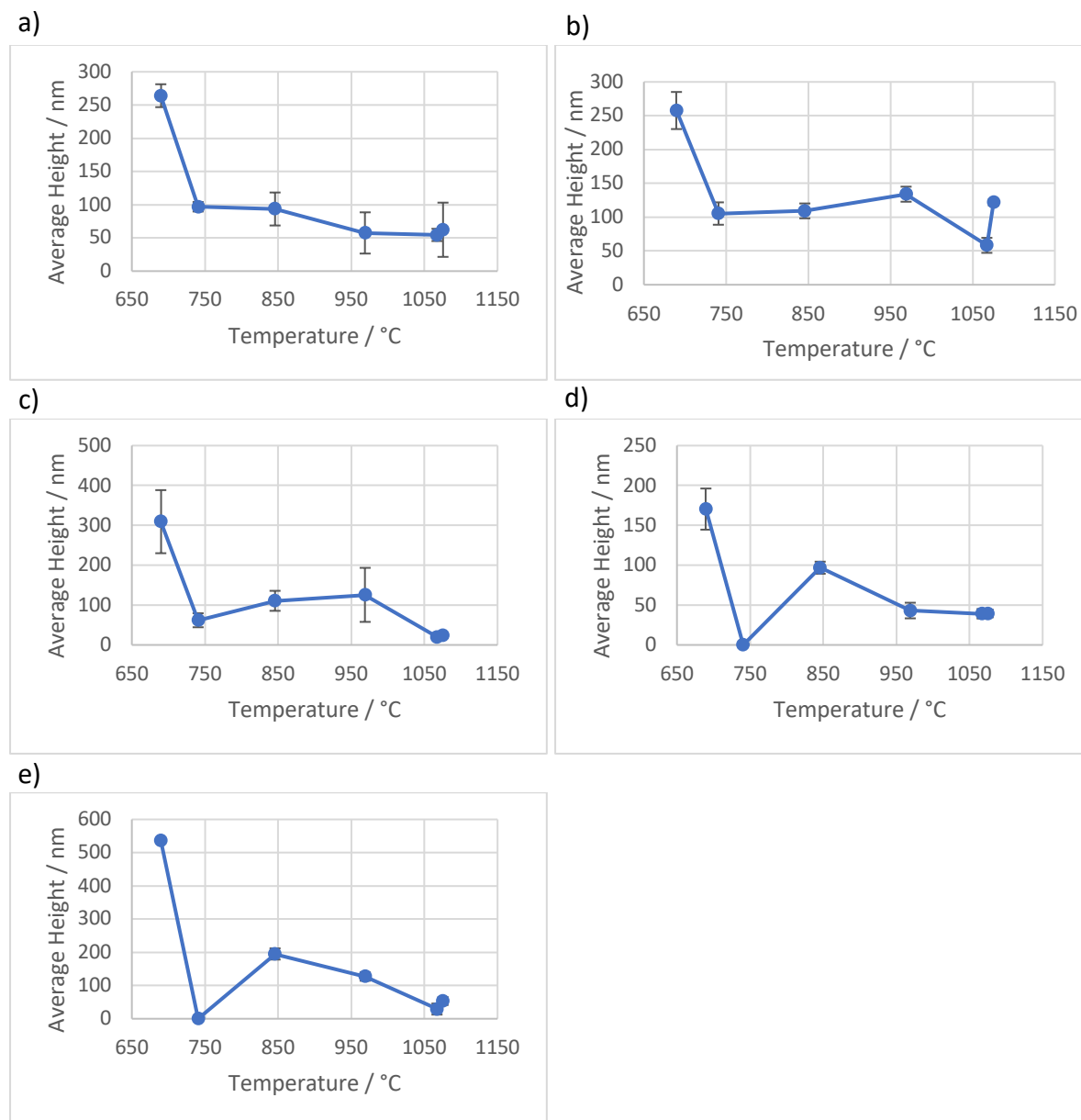


Figure 7: Graphs showing average nanostructure height for differing growth times a) 3 minutes b) 10 minutes c) 20 minutes d) 40 minutes e) 60 minutes.

There is a clear trend throughout the different growth times with, as expected, the 60 minutes of growth yielding the highest average structure heights. Generally, with some exceptions, as growth time increased so did structure height. All of the time intervals had an initial high average structure height at the lowest temperature compared to the higher temperatures. Is backed up by paper saying increased time=more growth.⁹

4. Conclusion:

It was found that at lower temperatures, there is a lot of graphitic deposition causing nanostructure height to be increased, however, these protrusions are not the desired product. Furthermore, it was found that at higher temperatures etching rates are increased leading to decreasing nanostructure heights. Therefore, there is a midpoint of temperature that allows for diamond deposition with the least amount of etching, yielding the diamond nanostructures with the greatest heights. This temperature, as shown by the graphs, lays between approximately 850-1000 °C. Alongside temperature, the growth times were explored, showing that an increase in time correlates to greater diamond growth.

5. Bibliography

1. M. V. Garciacuena, C. Serra, F. Lopez and J. L. Morenza, *Thin Solid Films*, 1991, **205**, 43-46.
2. Y. N. Palyanov, I. N. Kupriyanov, A. F. Khokhryakov and Y. M. Borzdov, *Crystengcomm*, 2017, **19**, 4459-4475.
3. P. W. May, *Philosophical Transactions of the Royal Society of London Series a-Mathematical Physical and Engineering Sciences*, 2000, **358**, 473-495.
4. W. Banholzer, *Surface & Coatings Technology*, 1992, **53**, 1-12.
5. Y. A. Mankelevich and P. W. May, *Diamond and Related Materials*, 2008, **17**, 1021-1028.
6. N. Jalili and K. Laxminarayana, *Mechatronics*, 2004, **14**, 907-945.
7. S. Morita, S. Fujisawa, E. Kishi, M. Ohta, H. Ueyama and Y. Sugawara, *Thin Solid Films*, 1996, **273**, 138-142.
8. K. E. Spear and M. Frenklach, *Pure and Applied Chemistry*, 1994, **66**, 1773-1782.
9. B. A. Reshi, S. Kumar, A. Misra and R. Varma, *Materials Research Express*, 2019, **6**, 046407.